Available online at www.sciencedirect.com
ScienceDirect
Journal of the European Ceramic Society 28 (2008) 241–246
www.elsevier.com/locate/jeurceramsoc

Indentation creep of free-standing EB-PVD thermal barrier coatings

V. Jan [a,*], F. Dorčáková [b], J. Dusza [b], M. Bartsch [c]

[a] *Toyota Technological Institute, 2-12-1 Hisakata Tempaku, Nagoya 468-8511, Japan*
[b] *Institute of Materials Research, Slovak Academy of Sciences, Watsonova 47, 04353 Košice, Slovak Republic*
[c] *Institute of Materials Research, German Aerospace Center (DLR), Linder Höhe, D-51147 Köln, Germany*

Received 7 November 2006; received in revised form 1 April 2007; accepted 20 April 2007
Available online 16 July 2007

Abstract

The indentation creep behavior of a free-standing 7 wt% Y-ZrO_2 thermal barrier coating (TBC) prepared by electron beam physical vapor deposition (EB-PVD) has been investigated. The specimens in the form of discs with 5 mm in diameter and 1.2 mm thickness were used for experiments in the temperature ranging from 1100 to 1300 °C and at stresses from 30 to 70 MPa, in air. A flat-ended cylindrical indenter has been used.

The strain–time relationship was recorded, and the creep exponents and activation energies of the creep have been calculated. The creep micromechanisms have been also studied by means of scanning electron microscopy.

The obtained creep stress exponent varied from 0.05 to 1.12 and the obtained activation energy in the interval from 215 to 329 kJ/mol. The main creep mechanisms are densification of the sub-layers with fine columnar crystals, bending of crystals and leaning down of sets of crystals.

Keywords: Creep; ZrO_2; Engine components; Thermal barrier coatings

1. Introduction

Thermal barrier coatings (TBCs) were developed for advanced gas turbines as insulating materials in order to maintain a substantial temperature difference between the load bearing alloy and the coating's surface. Usually they are formed by yttria stabilized zirconia (YSZ) applied by plasma spraying (P-S) or electron beam physical vapor deposition (EB-PVD). The challenge in developing new materials for TBCs with enhanced overall performance lies in the balance between improved thermal resistance and diminished durability.[1,2] Applying these coatings prolongs the lifetime of the components and allows higher turbine inlet temperature which results in improved efficiency of the system.[3]

Typically, a thermal protection system consist of four parts: the zirconia TBC, the super alloy substrate, an aluminum containing bond coat between the substrate and the TBC, and a thermally grown oxide layer formed between the TBC and the bond coat. Damage of any of these usually results in damage of the whole part.[4]

For interfacial fracture toughness of TBC systems, indentation techniques are often used.[5,6] Abrasion and adhesion tests are used, as the tolerance to impact of foreign objects and studying the cohesion of substrate and coating are of great importance.[7] The erosion rate and the susceptibility to delamination of the TBC system is affected by the plastic response of the top zirconia layer at elevated temperatures.[8,9] Recent tests[7,10] of different TBC's revealed susceptibility to heterogeneous deformation and crack formation in the columnar microstructure.

The creep tests of TBCs were realized by laser sintering and dilatometry[11,12]; also indentation/impression technique can be applied either to the whole TBC including the metallic substrate, or to a specially prepared system, e.g., a coating layer on a stiff substrate. Indentation creep has been originally introduced for measuring the viscosity of glasses; later the method was introduced for other materials.[13,14] In this test a cylinder (or cone/sphere) is pressed into the surface of a tested sample at a constant load and temperature; the impression depth as a function of time is registered. The creep curves resulting from these tests have a short initial transient stage, and then show a constant impression velocity. Comparing to conventional (tensile or compression) creep tests, the indentation creep test requires smaller samples of the tested material with only one flat surface adjusted perpendicularly to the indentation and provides higher

* Corresponding author. Tel.: +420541143187; fax: +420541143198.
E-mail address: jan@fme.vutbr.cz (V. Jan).

0955-2219/$ – see front matter © 2007 Elsevier Ltd. All rights reserved.
doi:10.1016/j.jeurceramsoc.2007.04.011

strain rates.[13,14] In order to compare the results of impression creep and those of uniaxial tensile test, the impression velocity, v_i, and the load, F, must be converted into equivalent tensile stress σ and strain rate $\dot{\varepsilon}$, by the following formulae:

$$\sigma = \frac{p}{k_1}, \qquad p = \frac{4F}{\pi d^2} \quad \text{and} \quad \dot{\varepsilon} = \frac{v_i}{k_2 d},$$

where p is the pressure just below the indenter and d is its diameter, k_1 and k_2 are material specific constants.[1,13,15]

It is not possible to realize a high-temperature indentation creep test of the TBC coating with a super alloy substrate in reliable way due to the deformation of the substrate. There are two possibilities as to how to avoid the deformation of the substrate: to apply the coating to a creep resistant substrate (e.g., alumina) or to use a free-standing TBC. Due to the character of EB-PVD-deposited material, the indentation creep tests have to be realized with stress applied perpendicular to the plane of deposition.

The aim of this work is to study the indentation creep behavior of a free-standing TBC material under different temperatures and loads in air and to investigate the creep mechanisms and creep damage under these conditions.

2. Experimental material and methods

The tested material was prepared at the DLR Köln, Germany. To be able to study the creep behavior, a material consisting of several consecutive layers of EB-PVD-deposited Y-ZrO_2 was prepared for this investigation. The investigated specimens were made as free-standing, so there was no substrate present during the test. The overall thickness of the samples was approximately 1.2 mm.

A flat cylindrical indenter with a diameter of 2 mm was used for the indentation creep tests. Monolithic SiC was used for the indenter and specimen support. This material has much higher creep resistance than that of the EB-PVD-deposited layer, so the measured values could be assumed to originate only from the coating's material (Fig. 1).

The specimens were heated to test temperatures in the range of 1100–1300 °C in air, and then stressed with the selected loads of 30, 50 and 70 MPa. The load remained unchanged during the test. Induction sensors connected to an input card in PC

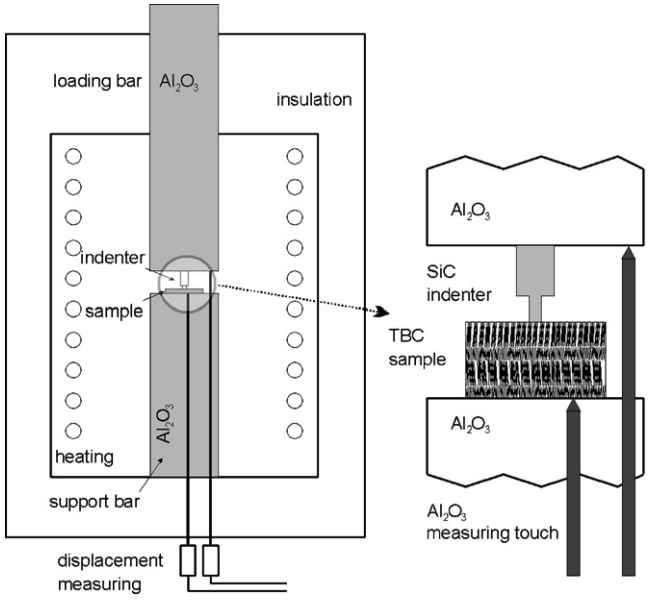

Fig. 1. The impression test configuration.

were used for measuring the immersion of the indenter into the specimen with an accuracy of 1 μm.

After the creep test, the load was removed from the specimen and the oven was left to cool slowly. The specimens were then broken in two parts and both fracture surfaces and polished sections were studied.

3. Results and discussion

3.1. Microstructure study of the as-received material

The as-received material consisted of three consecutive layers of EB-PVD-deposited crystals (Fig. 2a and b). The thickness of the layers varied between 200 and 500 μm. Each of the layers consisted of two sub-layers. The lower sub-layer is formed by fine crystals, which form sets that have a common point of crystal nucleation and have a thickness of about 30 μm (Fig. 2b). There is some porosity inside this sub-layer in the form of cracks with a length of approximately 20 μm between the wider bundles of small crystals with a width of approximately 10 μm. Above this sub-layer of fine crystals another sub-layer of coarse columnar

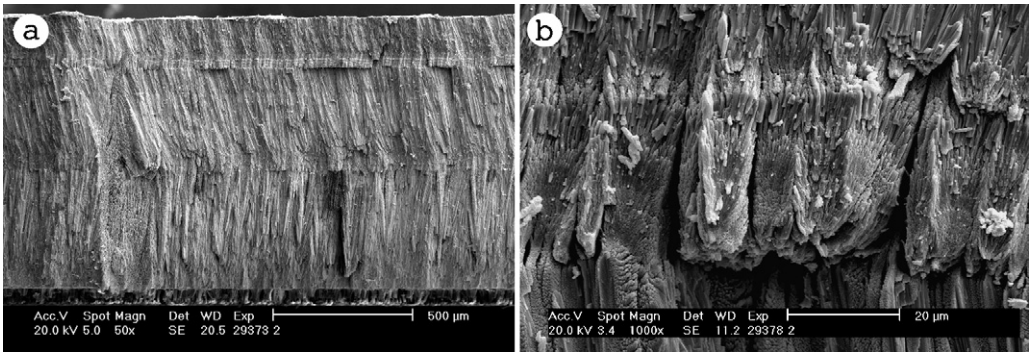

Fig. 2. (a, b) Non-deformed profile of the specimen—several layers with columnar crystals are visible (a) and detail of the non-deformed profile—the sub-layer of fine, shorter crystals (forming bundles) are visible (b).

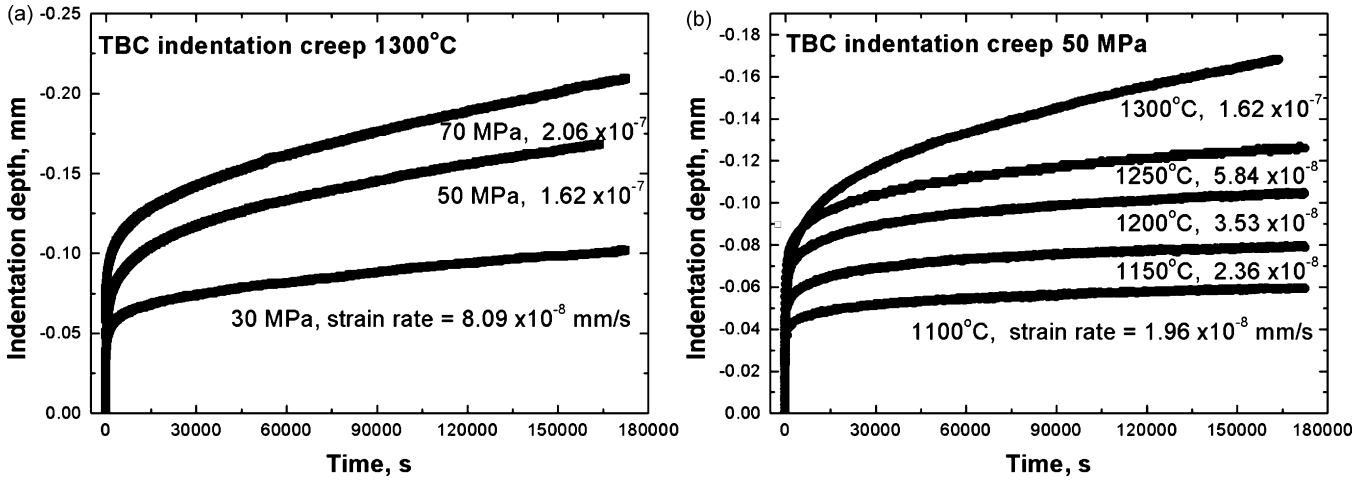

Fig. 3. Creep curves obtained at 1300 °C at stresses of 30, 50 and 70 MPa (a) and at 50 MPa stress at different temperatures (b). Strain rates are noted with the curves.

crystals is formed. The coarse crystals form the majority of the material thickness. The angle between the crystals main axis of different layers is approximately 5–10°.

3.2. Creep results

Indentation depth–time curves for different temperatures are illustrated in Fig. 3. According to the results, the creep deformation is minimal for temperatures in the interval from 1100 to 1200 °C and a reasonable deformation takes place only at the temperatures 1250 °C and higher. The strain rate (impression rate) is changing in the interval from 1.65×10^{-8} mm/s at temperature 1100 °C to 2.06×10^{-7} mm/s at 1300 °C. The values of strain rates systematically grow with higher temperatures and/or strains.

The calculated stress exponents are illustrated in Fig. 4. According to the results, the stress exponents are changing in the interval from 0.05 to 1.12. No influence of applied stress on strain rate was found at the temperature of 1100 °C with the calculated stress exponent of 0.05. At the temperature of 1200 °C the value of stress exponent was found still to be very low (0.42) and only for 1200 °C a value for the stress exponent higher than 1 was found.

Values of the activation energies (Fig. 5) are also low, varying in the interval from 215 to 329 kJ/mol. At all applied loads the activation energies are increasing non-linearly with increase of the testing temperature.

3.3. Microstructure study of the crept material

After the creep deformation, the indents could be observed on the polished sections (Fig. 6) and on the surface of the specimens (Fig. 7A) which remained in one piece in spite of the fact that some macrocracks were generated through the specimen.

Three different structural changes were identified in the deformed specimens. *First*, the lower part of each layer consisting of fine crystals with high porosity was compressed and the crystals were sintered to form what appears to be a compact layer (Figs. 6B and 7B). Fig. 7C and D shows the microstructure at the transition from the uncompressed porous layer of fine crystals to the compressed and sintered area and the non-deformed sub-layer far from the impressed area. This sintering

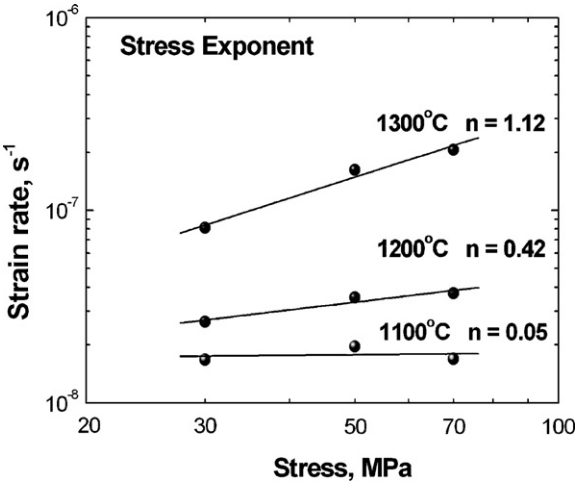

Fig. 4. Stress exponents calculated for the investigated temperatures.

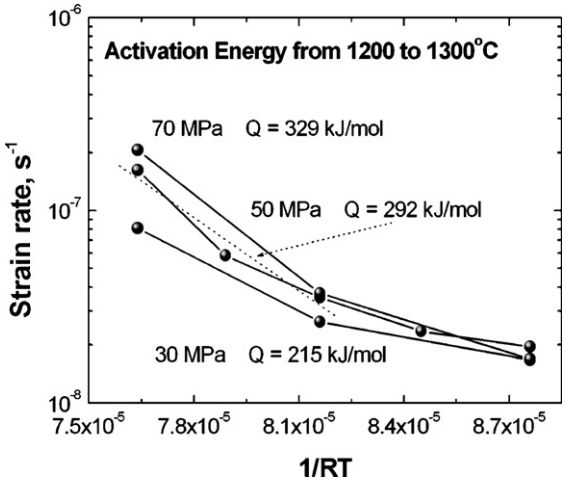

Fig. 5. The activation energy of creep deformation at stresses of 30, 50 and 70 MPa.

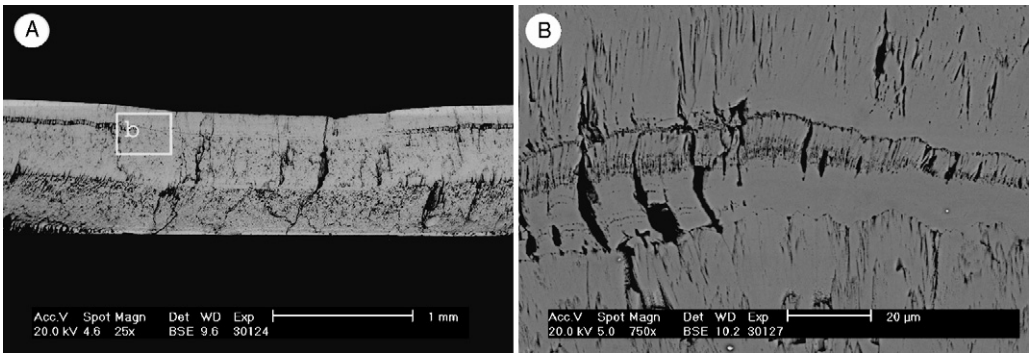

Fig. 6. Polished section of the deformed specimen, cracks and densifying of the base sub-layers are clearly visible below the indent (A). Detail of the sub-layer at base of the columnar crystals that is being densified (B).

type of densification mechanism was most evident at the highest testing temperature. The *second* mechanism was bending of the columnar crystals above the newly sintered layer (Fig. 8). This bending mechanism takes place more significantly at higher temperatures, but can be found also at 1100 °C. *Third*, the long stiff crystals, which form the majority of the TBC ceramic layers, did resist to the load very well, however, being not exactly parallel with the applied force, maintaining their individual shape, they slip and started to lean down resulting in further overall deformation of the specimen (Fig. 9).

3.4. Discussion

The creep behavior of a polycrystalline ceramics can be described by the following equation:

$$\dot{\varepsilon} = A\sigma^n L^{-p}[\mathrm{B}]P(\mathrm{O}_2)^m \exp\left(-\frac{Q_\mathrm{c}}{RT}\right),$$

where $\dot{\varepsilon}$ is the steady-state creep rate, σ the applied stress, n the stress exponent, L the grain size, p the grain size exponent, [B] the concentration of the rate-controlling defect, $P(\mathrm{O}_2)$ the oxygen partial pressure, m the oxygen partial pressure exponent, Q_c the activation energy for creep, A is a constant, T the absolute temperature and R is the gas constant.[10,16–18]

The activation energies and stress exponents obtained in this study are in the intervals of 215–329 kJ/mol and 0.05–1.12, respectively (Figs. 4 and 5). These values are low compared to the published values for the conventional zirconia measured using classical creep tests ($n \sim 1$–2, $Q \sim 460$ kJ/mol for sintered 8YSZ).[7,10,19–24] The activation energy values obtained for the

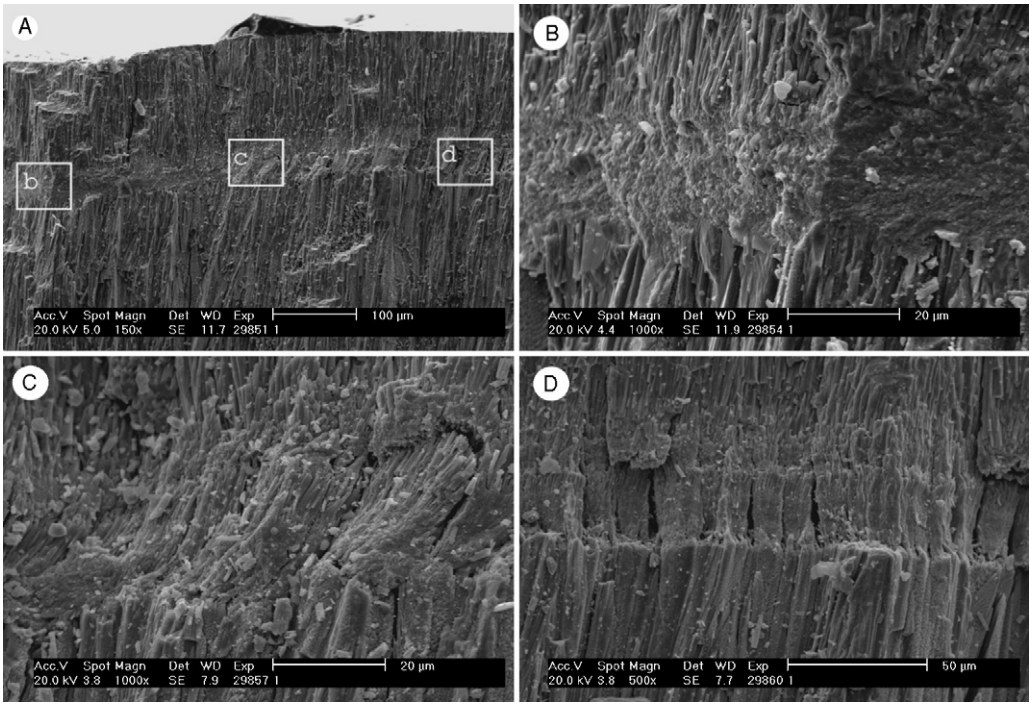

Fig. 7. Profile of the sub-layer at base of the columnar crystals that is being densified (cracked surface) (A), densified sub-layer (B), transition area with partly densified and leaned down small crystals (C), and fine crystals in the tested specimen far from the impressed area (D).

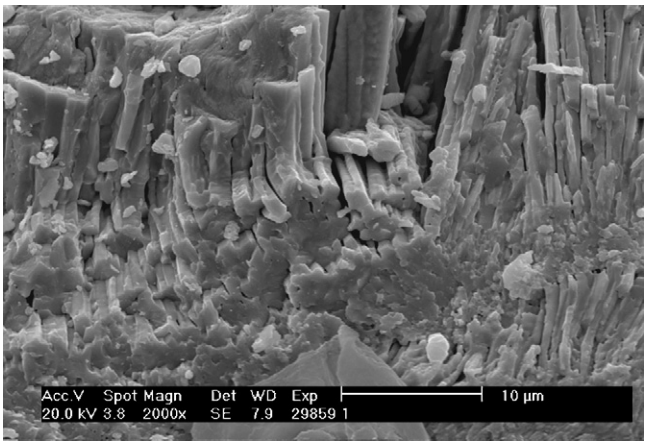

Fig. 8. Bending of the columnar crystals above the densified layer.

investigated material are also lower than activation energies for grain boundary diffusion.[10]

The creep of P-S TBCs has been investigated by different methods. Firestone et al.[12] show splat sliding as the main creep mechanism. Also sintering and creep of TBCs under compressive stresses at relatively low temperatures was reported. Zhu and Miller[11] used dilatometry to investigate the creep of different P-S TBCs. Materials with higher chemical and phase stability showed improved sintering/creep resistance.

The low-stress creep characteristics of the ceramic coating materials, determined by the dilatometer technique, are similar to the creep behavior of P-S TBCs obtained from high-temperature mechanical creep tests[3,14,22,26] and the laser sintering/creep test.[25]

Compressive creep test was used on the temperature interval from 900 to 1300 °C for characterization of the creep behavior of P-S ZrO_2 TBCs at stresses between 1.8 and 80 MPa by Thuru el al.[26] Beside the creep deformation, shrinkage of the material was observed leading to the change of its elastic properties. We have to note that due to the significantly different microstructure of the plasma sprayed ZrO_2 and EB-PVD ZrO_2 the creep mechanisms probably are significantly different, too.

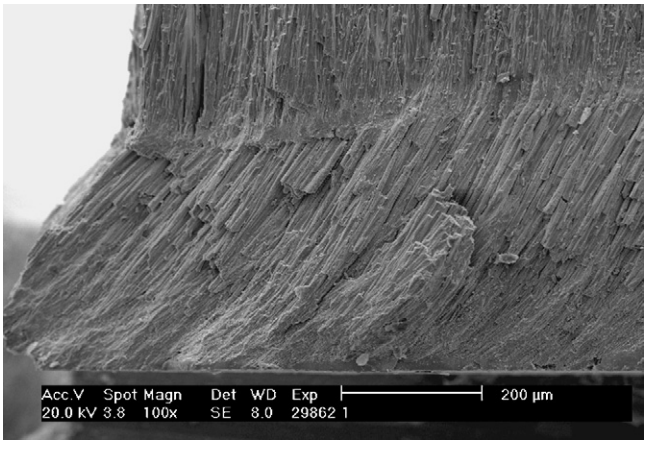

Fig. 9. Detail of the leaned down long crystals which were nonparallel to the applied force.

Recently Watanabe et al.[27] and Chen et al.[2] investigated the plastic deformation of EB-PVD thermal barrier oxides at high temperatures using impression technique also with stress applied perpendicularly to the plane of deposition. According to the results the penetration depth at the temperature of 1137 °C for the 7 wt% $Y_2O_3 + ZrO_2$ material at the applied stress of approximately 30 MPa is approximately 60 μm. Although they used a spherical indenter and therefore different deformation was induced in the material, some features may be compared with our experimental results. At the temperature of 1150 °C and load 50 MPa, the penetration depths of the cylinder were approximately 50 μm.

They also found a zone of deformation and densification below the indent at 1137 °C, with extreme plastic bending of crystals in the dense layer. This may be compared to our layers of bended and densified/sintered crystals.

4. Conclusions

Indentation creep tests of free-standing samples of 7-YSZ EB-PVD layers used as TBC topcoats were carried out at temperatures from 1100 to 1300 °C and stresses from 30 to 70 MPa, in air. The values of deformation exponent and activation energy are lower compared to the published values of the conventional bulk 8YSZ obtained using tensile creep test. This is most likely due to the different microstructure of the EB-PVD coatings in contrast to the sintered materials, but probably also due to the different testing procedure. The values for strain rate and indentation depths can be considered to be in an agreement with values reported by other authors for similar tests of EB-PVD coatings. The microstructure analysis of the deformed samples allowed identifying three mechanisms that undergo during the indentation creep test. These include sintering of fine crystals, bending of bigger columnar crystals and leaning down of columnar crystals, which were not parallel to the applied force.

Acknowledgements

The work was supported by the European Community's Human Potential Programme under contract HPRN-CT-2002-00203 [SICMAC], by NANOSMART, Centrum of Excellence of SAS, Slovak Grant Agency for Science via grant No. 2/4173/04 and by the Science and Technology Assistance Agency under the contract No. APVT-51-049702.

Vít Jan acknowledges the financial support provided through the European Community's Human Potential Programme under the contract HPRN-CT-2002-00203 [SICMAC] and of Grant Agency of Czech Republic under GACR 106/07/P198.

Jan Dusza acknowledges the support of the Alexander von Humboldt Foundation.

References

1. Miller, R. A., In *Proceedings of the Thermal Barrier Coatings Workshop*, 1995, pp. 17–34.
2. Chen, X., Hutchinson, J. W. and Evans, A. G., *Acta Mater.*, 2004, **52**, 565–571.

3. Stiger, M. J., Yanar, N. M., Topping, M. G., Pettit, F. S. and Meier, G. H., *Z. Metallknd.*, 1999, **90**(12), 1069–1078.
4. Evans, A. G., Mumm, D. R., Huntchinson, J. W., Meier, G. H. and Pettit, F. S., *Prog. Mater. Sci.*, 2001, **46**, 505–553.
5. Vasinota, A. and Beuth, J. L., *Eng. Fract. Mech.*, 2001, **68**, 843–860.
6. Bartsch, M., Mircea, I., Suffner, J. and Baufeld, B., *Key Eng. Mater.*, 2005, **290**, 183–190.
7. Chokshi, A. H., *J. Eur. Ceram. Soc.*, 2002, **22**, 2469–2478.
8. Bruce, R. W., Development of 1232_C (2250 F). *Tribol. Trans.*, 1998, **41**(4), 399–410.
9. Chen, X., Wang, R., Yao, N., Evans, A. G. and Hutchinson, J. W., *Mater. Sci. Eng. A*, 2003, **352**(1–2), 221–231.
10. Wolfenstine, J., *J. Power Sources*, 2002, **111**, 173–175.
11. Zhu, D. and Miller, R. A., *Surf. Coat. Technol.*, 1998, **108–109**, 114–120.
12. Firestone, R. F., Logan, W. R., Adams, J. W. and Bill, R. C. J., In *Proceedings of the Sixth Annual Conference on Composites and Advanced Ceramic Materials*, ed. J. D. Buckley, C. M. Packer and J. J. Gebhardt, 1982, p. 758.
13. Cseh, G., Bar, J., Gudladt, H.-J., Lendvai, J. and Juhasz, A., *Mater. Sci. Eng. A*, 1999, **272**, 145–151.
14. Li, J. C. M., *Mater. Sci. Eng. A*, 2002, **322**, 23–42.
15. Tchizhik, A. A., Getsov, L. B., Rybnikov, A. I. and Malashenko, I. S., *Thin Solid Films*, 1995, **270**, 243–246.
16. Pascoe, R. T. and Hay, K. A., *Philos. Mag.*, 1973, **27**, 897.
17. Dominquez-Rodriquez, A., Monty, C. and Philibert, J., *Philos. Mag. A*, 1982, **46**, 869.
18. Wolfenstine, J. and Kohlstedt, D. L., *J. Mater. Sci.*, 1988, **23**, 3550.
19. Evans, P. E., *J. Am. Ceram. Soc.*, 1970, **53**, 365.
20. St-Jacques, R. G. and Angers, R., *J. Am. Ceram. Soc.*, 1972, **55**, 571.
21. Dimos, D. and Kohlstedt, D. L., *J. Am. Ceram. Soc.*, 1987, **70**, 531.
22. Wakai, F., *Acta Metall. Mater.*, 1994, **42**, 1163.
23. Wolfenstine, J., Huang, P. and Petric, A., *Solid State Ionics*, 1999, **118**, 257–259.
24. Wolfenstine, J., *Electrochem. Solid State Lett.*, 1999, **2**, 210.
25. Ahmaniemi, S., Vuoristo, P. and Mantyla, T., *Mater. Sci. Eng. A*, 2004, **366**, 175–182.
26. Thuru, G., Schneider, G. A. and Aldiger, F., *Mater. Sci. Eng. A*, 1997, **233**, 176–182.
27. Watanabe, M., Mercer, C., Levi, C. G. and Evans, A. G., *Acta Mater.*, 2004, **52**, 1479–1487.